# Effect of indium (III) doping on $Ag_3PO_4$ catalyst stabilization and its visible light photocatalytic activity toward toxic dyes

Habiba Khiar[1], Fatima Zahra Janani[1], M'hamed Sadiq[1], Said Mansouri[2], Alberto Puga[3], Noureddine Barka[1,*]

[1] Sultan Moulay Slimane University of Beni Mellal, Multidisciplinary Research and Innovation Laboratory, FP Khouribga, BP. 145, 2500 Khouribga, Morocco.

[2] Materials Science Energy and Nanoengineering Department (MSN), Mohammed VI Polytechnic University (UM6P), Lot 660-Hay Moulay Rachid, 43150 Benguerir, Morocco

[3] Departament d'Enginyeria Química, Universitat Rovira i Virgili, Avinguda dels Països Catalans, 26, 43007 Tarragona, Spain.

[*] Corresponding author: barkanoureddine@yahoo.fr

## Abstract

Indium(III)-doped $Ag_3PO_4$ (In-AgP) catalysts with different weight percentages were elaborated by co-precipitation and characterized by XRD, SEM, DRUV-vis and FTIR. The prepared catalysts are of spherical morphology and their diameters differ with doping. The whole materials crystallize in a centered cubic system with a slight dissimilation in the positions of the characteristic peaks as function of indium dosage. The photocatalytic performance of the catalysts was studied for the photocatalytic degradation of anionic dye (methyl orange (MO)) and cationic dye (auramine O (AO)) in moderate acid (pH=4), neutral (pH=7), and basic (pH=10) conditions under visible light irradiation. Results showed more selectivity to MO than AO. Furthermore, indium doped samples are more active in the acidic medium than, and 10%In-AgP present the highest activity. The degradation efficiency reached 99% in short time duration, and high recycling stability was achieved so the catalyst retains its degradation capacity above 99% after five cycles.

**Keywords**: Indium doped silver phosphate; Photocatalyst reusability; Stabilization; Dyes removal.

## 1. Introduction

With the increase of environmental issues related to the emergence of toxic chemicals in wastewaters, the researchers dive hardly to develop ecofriendly processes for the degradation of these emerging contaminants before being released in the receipt environment [1]. Since its discovery in early 1970s by Fujishima and Honda [2] semiconductor photocatalysis gained a

huge reputation in tackling with environmental pollution. This technology has been greatly developed following this pioneering work not only in pollution remediation but also attain hydrogen and dioxygen production, bacteria disinfection and other purposes [3].

$TiO_2$ was the first semiconductor that Fujishima and Honda worked on and found that it can decompose water to produce oxygen and hydrogen under ultraviolet irradiation. Since then, $TiO_2$ was the subject for many other studies. However, with a large band gap, $TiO_2$ could be excited only by wavelength shorter than 400 nm which constitutes only 4-5% of the solar energy spectrum. So, the need for a visible light active material is really of big challenge in order to use directly the solar irradiation instead of pollutant fossil fuel sources to produce electricity. Many strategies have been adopted to target visible light active materials, either by modification of $TiO_2$ such as doping with certain metals, the case of $xCo/TiO_2$ [4], $Pt\text{-}TiO_2$ [5], V-doped $TiO_2$[6] or by integration $TiO_2$ in composites like $C_3N_4–TiO_2$ [7], $TiO_2\text{-}SiO_2$ [8], and graphene-$TiO_2$ [9]. Over time, further researches have been undertaken to develop new catalysts active under visible light and independent of $TiO_2$, for instance, BiOX (X=Cl, Br, I) [10], $MoS_2$-g-$C_3N_4$ [11], $Bi_2WO_6$ [12], $Ag_3VO_4$ [13] among others.

In 2010, Yi and coworkers reported the use of silver phosphate ($Ag_3PO_4$) as a highly active catalyst under visible light irradiation in water oxidation and organic contaminants degradation [14]. Nevertheless, large scale application is still a challenge for this semiconductor considering its instability when exposed to light. In order to boost the activity of $Ag_3PO_4$ and enhance its stability, many approaches have been undertaken, among them, the integration of $Ag_3PO_4$ in composites with different types of materials such as $CuBi_2O_4$ [15], $Co_3O_4$ [16], ZnO [17], g-$C_3N_4$ [18], chitosan [19], $BiPO_4$ [20], AgX (X= Cl, Br, I) [21] , polyaniline [22], and graphene [23].

Metal ion doping might be another competitive method in reducing the band gap width of the semiconductor and enhancing its stability. Cation elements that have been already used in $Ag_3PO_4$ doping are Bi [24], Ni[25], [26], Mo [27], W [28], Ba [29], La [30], Mn [31], Gd [32], [33], Dy and Er [32]. All these elements showed satisfactory results in boosting the visible light activity of silver phosphate and its stability. Doping with indium $In^{3+}$ cations has not been reported before, knowing that the element indium (Z = 49) is close to silver (Z = 47) in atomic number and that the radius of $In^{3+}$ is smaller than that of $Ag^+$, it could easily replace it.

In this work we have synthesized for the first time a series of indium(III)-doped $Ag_3PO_4$ using different percentages (5, 10, 15, and 20%) of indium ($Ag_{(3-3x)}In_xPO_4$). The structure and composition of elaborated materials were studied using different characterization methods. The

photocatalytic performance was tested on methyl orange and auramine O dyes photodegradation under visible light in different pH conditions.

## 2. Experimental

### 2.1. Materials

The chemicals used in this research are silver nitrate $AgNO_3$ (100.5%), sodium phosphate dibasic $Na_2HPO_4$ (98-100.5%), Indium (III) chloride $InCl_3$ (98%), methyl orange ($C_{14}H_{14}N_3NaO_3S$, 100%), and auramine O ($C_{17}H_{21}N_3HCl$; 85%). All these chemicals were bought from Sigma Aldrich (Germany) and were used without further purification.

### 2.2. Synthesis

Undoped $Ag_3PO_4$ (AgP) and In-doped $Ag_3PO_4$ (In-AgP) samples were prepared by a simple co-precipitation. In a typical experiment, 0.005 mol of sodium phosphate dibasic ($Na_2HPO_4$) and 0.010 mol of silver nitrate ($AgNO_3$) were dissolved in 50 mL of distilled water each. The aqueous solution of $Na_2HPO_4$ was added dropwise to $AgNO_3$ solution and kept under agitation for 60 min. Then, the precipitate was collected and washed several times until its pH remained constant and dried overnight at 80 °C in a vacuum oven. Finally, after crushing and sieving the powder was calcinated at 150°C to obtain $Ag_3PO_4$ sample. It is worthy to mention that this calcination temperature was not taken arbitrarily, we tried several temperatures: 150, 300, 400, and 500°C and even the uncalcined sample was tested, however, the material calcined at 150°C gave better photocatalytic results than others. For samples of x% In-doped $Ag_3PO_4$ (x = 5, 10, 15, 20) where x% represents the weight concentration percentage (wt.%), corresponding amounts of indium (III) chloride were added to $AgNO_3$ solution and the other steps were kept the same as for the synthesis of pristine $Ag_3PO_4$.

### 2.3. Characterization

To study the crystal phase and size, powder X-ray technique was applied using Empyrean, Spinner reflection-transmission configuration - Malvern Panalytical apparatus (CuKα, λ = 1.54 A°, 45 kV and 40 mA). A SCO TECH (SP-FTIR-1) spectrophotometer with KBr pellets was used to define functional groups in the range of 4000-400 $cm^{-1}$. The microstructure was determined using SEM/EDX (TECNAI G2/FEI) instrument, at an accelerating voltage of 120 kV. The optical properties were studied using UV-Vis diffuse reflectance spectra (DRS) measured on a Perkin Elmer PE 1050 device. The dye concentration was determined from UV-visible absorption characteristics using a UV-Vis TOMOS spectrophotometer (V-1100).

### 2.4. Photocatalytic activity experiments

The photocatalytic activity of the In-doped $Ag_3PO_4$ catalysts was compared to that of the undoped $Ag_3PO_4$ in the degradation of MO and AO under different aqueous solution pH (pH=4, pH=7, and pH=10). The photocatalytic tests were held in a homemade reactor, in a typical experiment, 100 mL of the dye solution with a concentration of 10 mg/L was mixed with 0.02 g of catalyst and kept under stirring for 1h in the dark to reach adsorption equilibrium. Then, the mixture was irradiated using a 250 W metal halide lamp and maintained under stirring. After an appropriate reaction time, samples were extracted, filtered and the residual dye concentration was determined.

## 3. Results and discussion

### 3.1. XRD analysis

Fig. 1 exhibited the XRD patterns of pure $Ag_3PO_4$ and In-doped catalysts. The diffraction peaks of $Ag_3PO_4$ indicated by the peaks at 2θ = 20.93°, 29.78°, 33.41°, 36.71°, 42.66°, 47.98°, 52.89°, 55.26°, 57.51°, 61.92°, 66.14°, 70.23°, 72.22°, 74.19° and 78.08°. These peaks correspond to the reflections from (110), (200), (210), (211), (220), (310), (222), (320), (321), (400), (330), (420), (421), (332), and (422) planes, respectively, are indexed to body-centered cubic system according to JCPDS card no. 06-0505 [34].

For In-doped $Ag_3PO_4$ material, three additional peaks at 27.87°, 32.31° and 46.41° were observed. These peaks can be assigned to (111), (200), and (220) reflections of the cubic AgCl (JCPDS card No. 31-1238) [35]. The figure also shows that the AgCl/$Ag_3PO_4$ portion increases with increasing $InCl_3$ precursor. This means that part of the silver reacts with the chloride ions to form AgCl material.

The crystallites size is estimated using the Scherrer's equation:

$$D = \frac{k\lambda}{\beta cos\theta}$$

where D is the crystallites size in nm, λ represent the x-ray wavelength (λ=0.15406 nm), k is a constant equal to 0.9, θ is scattering angle in radians, and the last parameter β is the FWHM in radians. For undoped and In-doped $Ag_3PO_4$ the crystallite sizes are 66.62, 50.94, 49.13, 46.06, and 39.36 nm for AgP, 5% In-AgP, 10% In-AgP, 15% In-AgP and 20% In-AgP, respectively. The crystallite size decreases, when the amount of In doping increased from 0% to 20%. This

result can be related to the incorporation of smaller In instead of Ag with an ionic radius of 0.081 Å and 0.155 Å respectively, within $Ag_3PO_4$ structure.

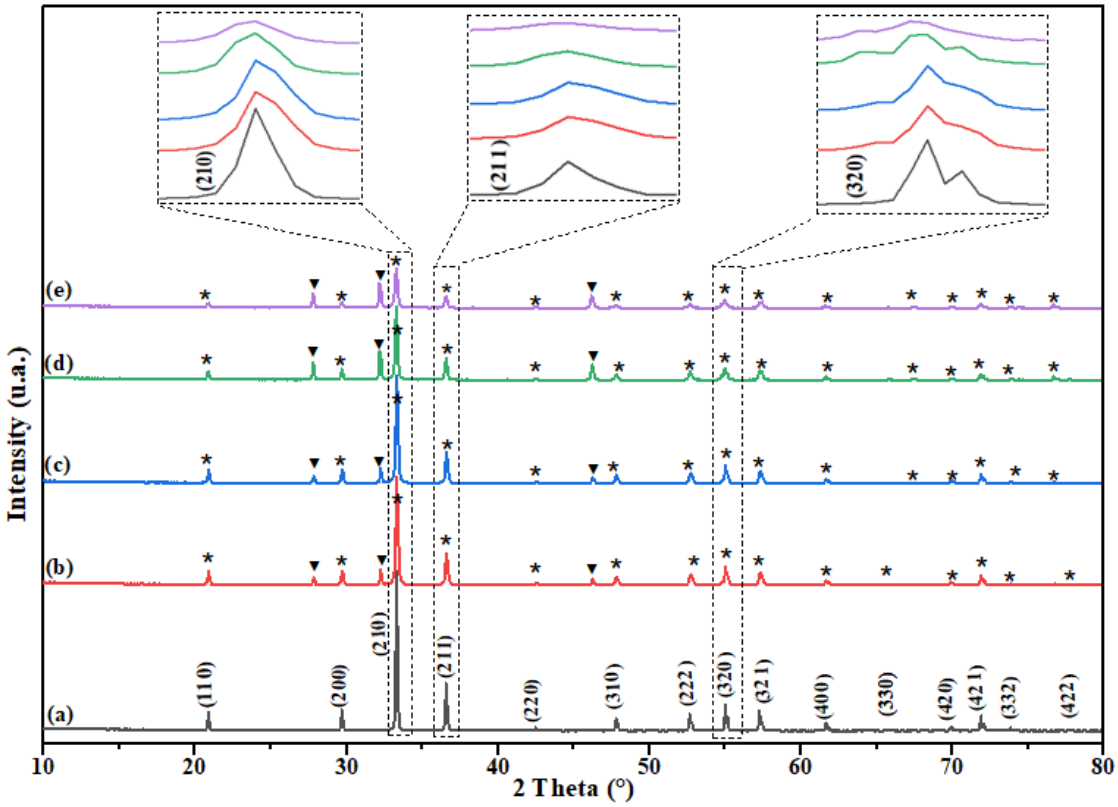


**Fig.1.** XRD patterns of (a) pure $Ag_3PO_4$, (b) 5%In-$Ag_3PO_4$, (c) 10%In-$Ag_3PO_4$, (d) 15%In-$Ag_3PO_4$, (e) 20%In-$Ag_3PO_4$; (*) $Ag_3PO_4$, (▼) AgCl

### 3.2. SEM analysis and elemental composition (EDX)

Particles morphology and size are factors directly influencing on the photocatalytic activity of $Ag_3PO_4$ catalysts [34]. These factors are themselves closely related to the used precursors. Fig.2 shows SEM images of undoped and $In^{3+}$ doped AgP synthesized using $AgNO_3$, $Na_3HPO_4$ and $InCl_3$ as starting reagents. All samples are composed of irregular spherical poreless particles. This morphology is largely found in so many other studies related to the synthesis of silver phosphate [35]–[38]. It is noteworthy to mention that pure AgP contains the largest particles size with an average diameter of 346.29 nm. As the dosage of $In^{3+}$ substitution increases, the diameter reduced to attain 58.68 nm for 10 %In-AgP, then starts to increase to reach 232.49 nm for 20%In-AgP, Table S1 in the supplementary materials represents the different average diameters estimated using ImageJ and Origin version 2018 softwares. Compared with the doped samples, AgP nanoparticles are agglomerated during the synthesis. Conversely, with the increase of doping, the grains are separated from each other. In parallel, small particles clearly cover the surfaces of the spheres in the 15 and 20% doped

samples (images (D) and (E) of Fig.2). These particles are present in large quantities in the latter compared to that doped with 15%, and their diameters varied between 39.1 and 41.77 nm, they might refer to the second phase (AgCl). SEM images are supported by elemental analysis showed on EDX spectra. Phosphorus (P), silver (Ag) and oxygen (O) are present in the samples, as well as the presence of indium is confirmed and the affected signals coincide with those of Ag beside the apparition of weak new ones at higher loading percentages, which confirm that $In^{3+}$ are present in AgP matrix and occupy $Ag^{+}$ sites. Even though, XRD confirms the presence of AgCl phase in the In-loaded samples, Cl element appears just in 5% In-AgP EDX spectra.

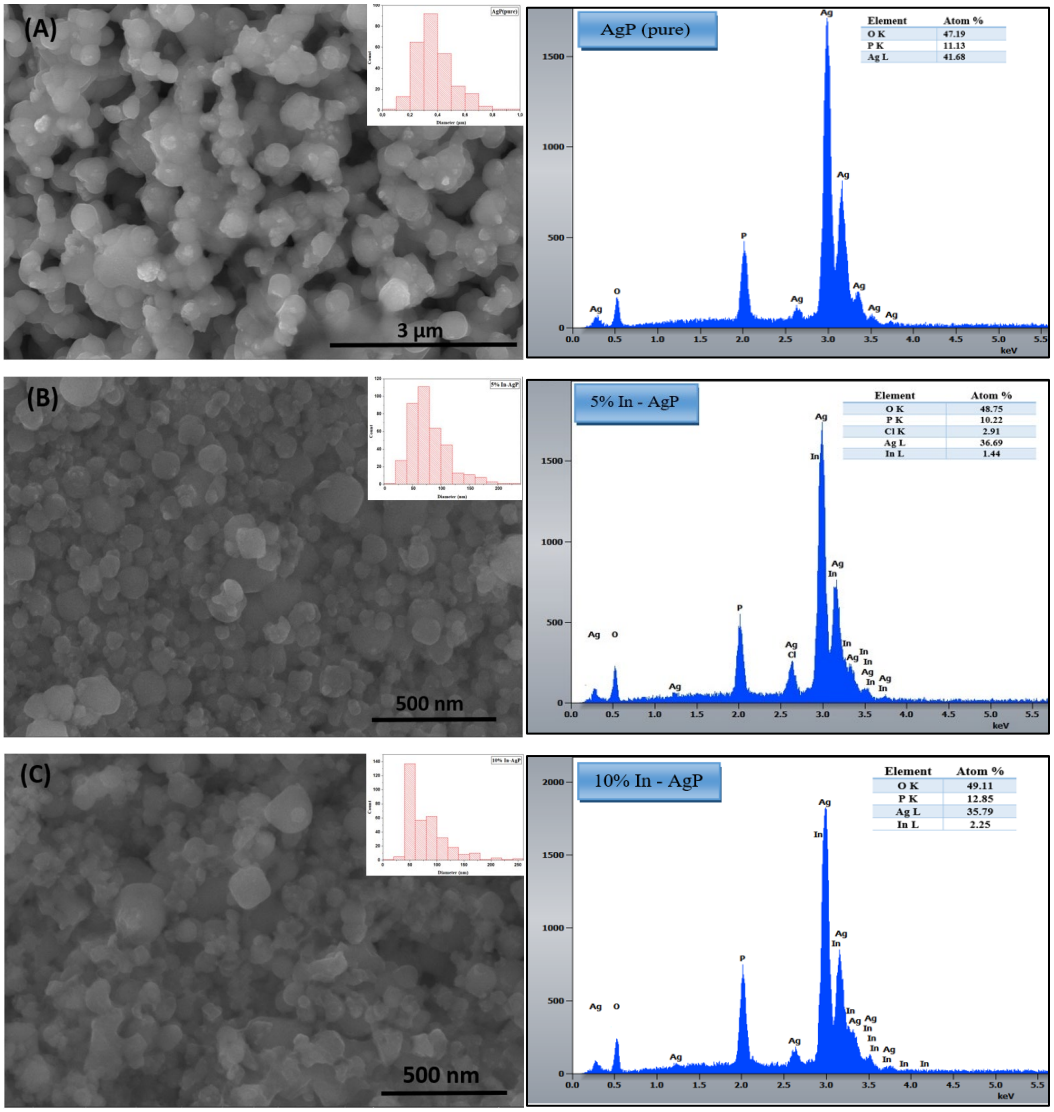

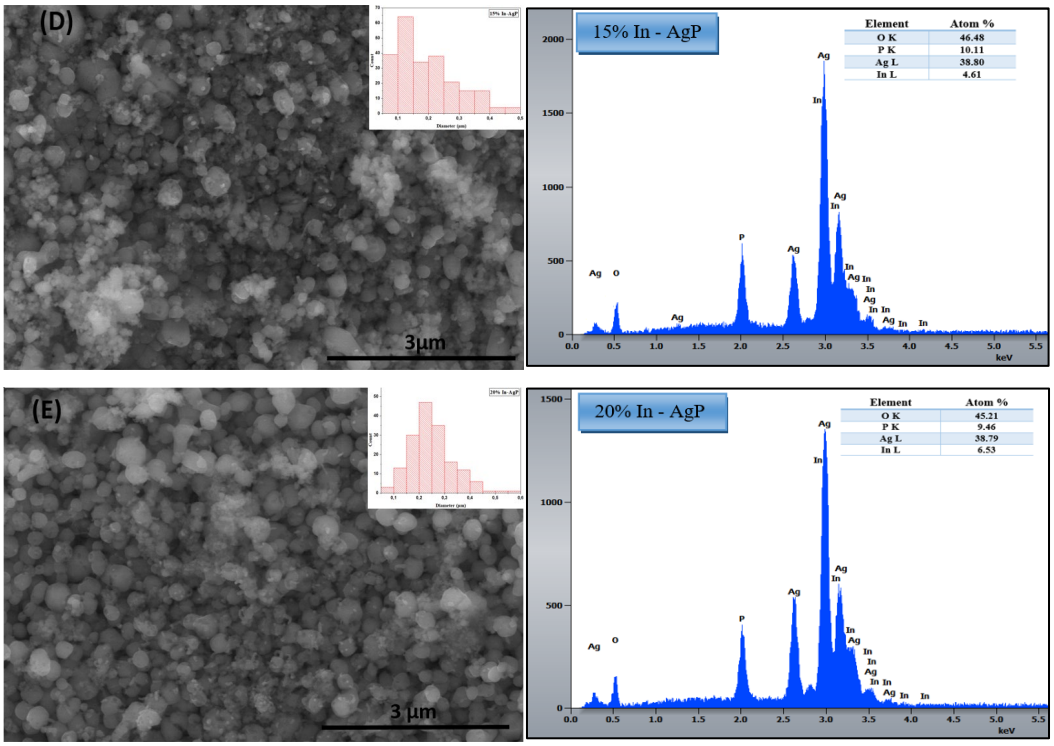


**Fig.2.** SEM/EDX of (A) $Ag_3PO_4$, (B) 5%In-$Ag_3PO_4$, (C) 10%In-$Ag_3PO_4$, (D) 15%In-$Ag_3PO_4$, (E) 20%In-$Ag_3PO_4$

### 3.3. FTIR analysis

Fig.3 depicts the FTIR spectra of pristine and In (III) doped AgP at different percentages. The spectra part between 400 and 1300 $cm^{-1}$ represents the characteristic vibrations of silver phosphate. The bands of indium doped AgP incur intensities changing and wavenumbers shifting compared to the undoped ones. For pristine AgP sample, the strong band at 1020 $cm^{-1}$ and the band at 722 $cm^{-1}$ are associated to the stretching vibrations of P-O-P groups of $PO_4^{3-}$ ions [24], [34]–[36], [39], [40]. Moreover, an intense peak at 551 $cm^{-1}$ could be assigned to asymmetric and symmetric stretching of O=P-O [36], [40]. In addition a weak peak at 440 $cm^{-1}$ is ascribed to $HPO_4^{2-}$ vibrational mode [39]. O-H stretching vibration of physically adsorbed water are presented by the broad absorptions at around 2500-3400 $cm^{-1}$, 1668 $cm^{-1}$ and 1387 $cm^{-1}$ [24], [39], [40]. We can clearly observe that the large absorption band between 2500 $cm^{-1}$ and 3400 $cm^{-1}$ plummeted with increasing doping and reach a minimum intensity at 10 wt% In-AgP. According to previous reports the FTIR peak area is proportional to the concentration of OH defects [39], [41]. This means that 10% In-AgP contains the minimum concentration of OH defects.

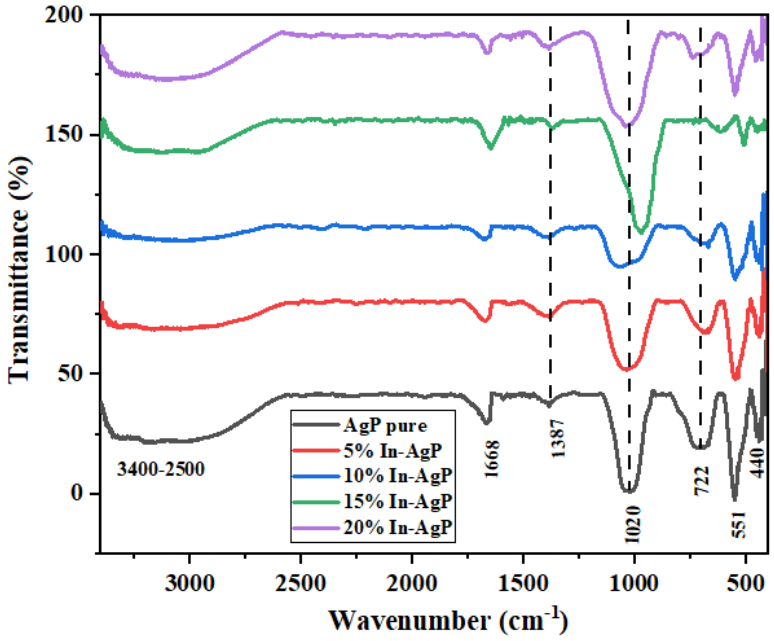


**Fig.3.** FTIR patterns of as prepared samples

3.4. Optical properties (UV-Vis DRS)

In order to investigate the optical properties of AgP before and after $In^{3+}$ doping, diffuse reflectance UV-Vis spectroscopy (DRS) was performed for pure phase AgP and In-doped AgP. The results are displayed in Fig.4. To elucidate the bandgap and assuming that $Ag_3PO_4$ is an indirect bandgap semiconductor, we used the famous Tauc-Mott formula:

$$(\alpha h\upsilon)^{1/2} = A(h\upsilon - Eg)$$

where α, h, υ, and A are respectively the absorption coefficient, Planck constant, light frequency, and proportionality constant. The energy gap was deduced from the plot of $(\alpha h\upsilon)^{1/2}$ as a function of hυ.

The pure AgP phase exhibits absorption of wavelengths below 450 nm. When AgP is doped with $In^{3+}$ the absorption edges have undergone a slight shift towards wavelengths shorter than that of the undoped sample, the absorptions of the different samples are lower than 420, 425, 435, 432 nm respectively for 5% In-AgP, 10% In-AgP, 15% In-AgP and 20% In-AgP. Even if the absorption is shifted towards the lower wavelength, the percentages of absorption are very important compared to the pure material. The decrease in the absorption wavelength supports the observed regression of the photocatalytic activity of silver phosphate. The bandgap energy estimate of the undoped sample and those of the samples doped with 5, 10, 15 and 20% $In^{3+}$ are 2.41, 2.67, 2.66, 2.32, and 2.58 eV, respectively. Obviously, the introduction of $In^{3+}$ into the lattice of AgP affected its valence and conduction band positions.

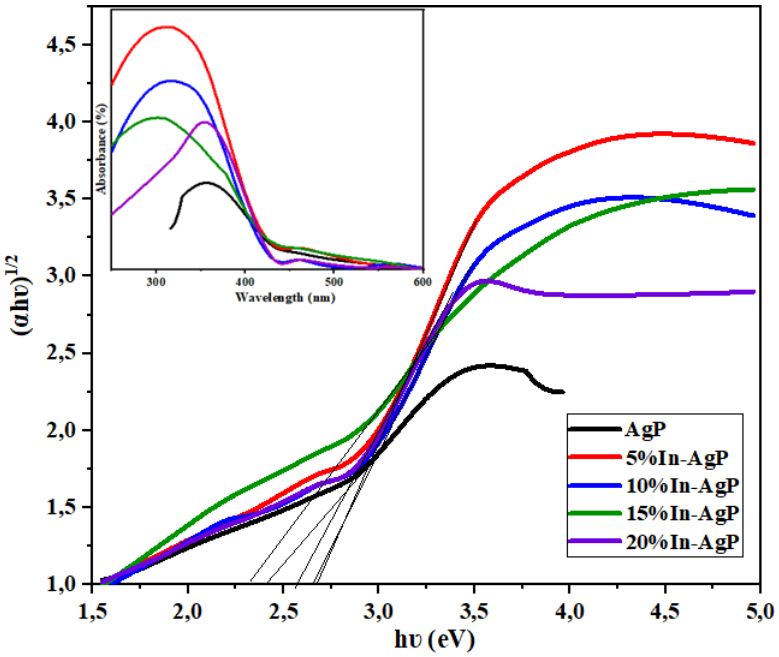


**Fig.4.** UV-Visible absorption spectra of AgP and In-doped AgP

### 3.5. Photocatalytic activity evaluation

The effect of $In^{3+}$ doping on the photocatalytic performance of AgP was evaluated in the degradation of MO and AO at neutral (pH=7), alkaline (pH=10), and moderate acid (pH=4) solutions. The other parameters such as temperature, pressure, mass of catalyst and dye concentration were kept constant during the whole tests, for the first two parameters, they were not changed from ambient conditions. Regarding the photocatalyst mass, it was maintained at 200 mg/L, and as for the dye solution, it was maintained at 10 mg/L.

Before the photocatalytic tests were carried out, the mixture of the dye solution and the solid was stirred for 1h in the dark to reach adsorption equilibrium. A photolysis test for both dyes in the different pH conditions was taken in absence of any catalyst. The obtained results show that the concentrations stay constant with increasing the irradiation time, which means that there is no decrease in the concentration of the dyes in absence of catalysts.

To study the photodegradation rate, we assume that the reactions follow a pseudo-first order kinetics that obey the following equation:

$$Ln(C_t/C_0) = - k_{obs}\, t$$

Where, $C_0$ is the initial dye concentration (at t=0), $C_t$ represents the concentration at time t and $k_{obs}$ is the pseudo-first-order rate constant ($min^{-1}$), it represents the slope of the straight line of $Ln(C_t/C_0)$ against the time of the degradation t. The different rate constants are shown in Table S2 in the supplementary materials.

### 3.5.1. Preliminary adsorption in the dark

The adsorption capacity of the different catalysts prepared was tested separately from the photodegradation under the same conditions mentioned above. Kinetic studies are shown in Fig.5. The conclusions that can be drawn from the graphs are that the adsorption of the materials behaves differently towards methyl orange than towards auramine O. In addition, at neutral pH there is no adsorption observed for MO, on the contrary AO is slightly adsorbed on the catalysts with a negligible quantity range from 5% to 10%. In an acidic medium, the two dyes are adsorbed within the limit of 10%. Concerning the pH 10, the AO obeys the adsorption capacity of the catalyst much more and reaches 22% for AgP and 18% for 15% In-AgP, however, a maximum of 10% of MO could be adsorbed.

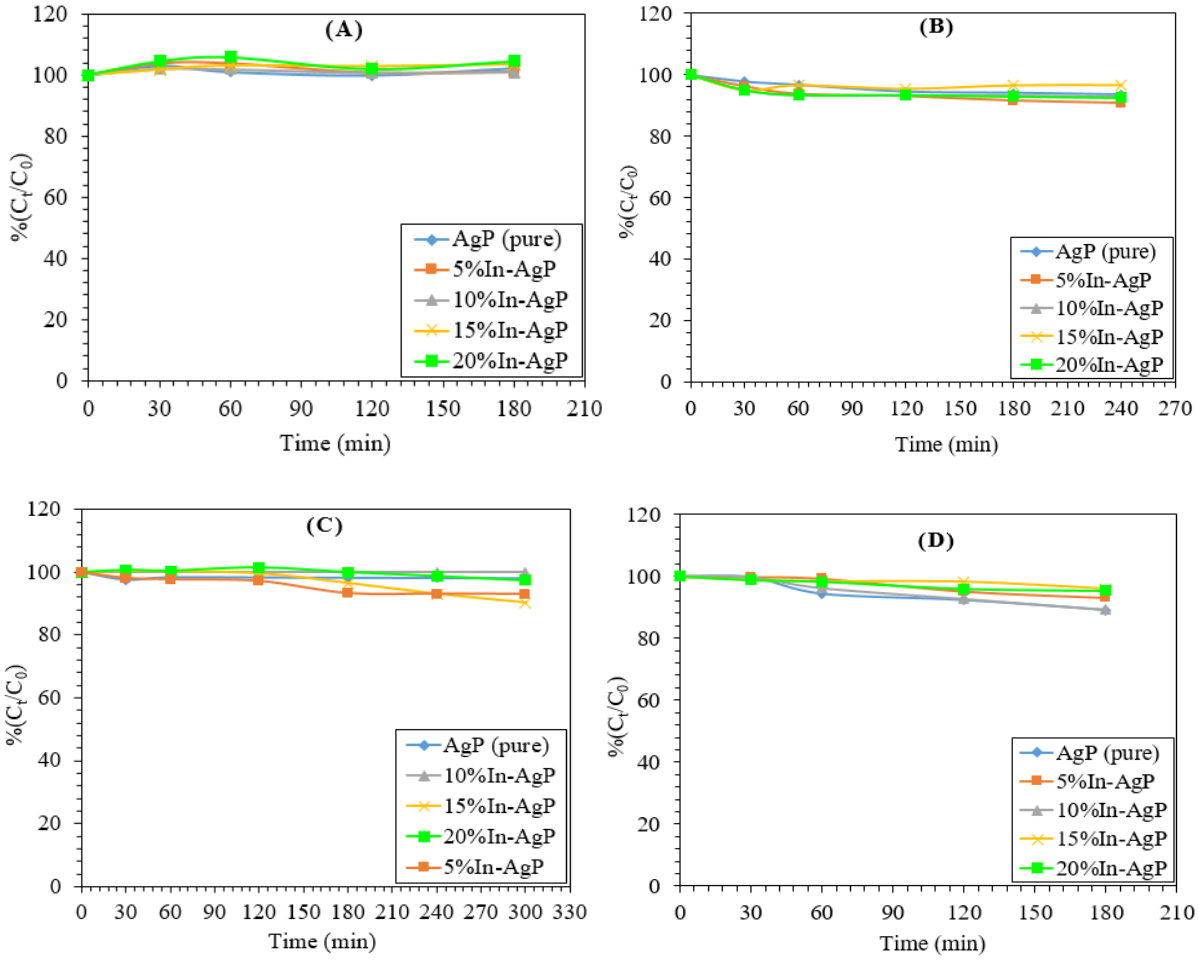

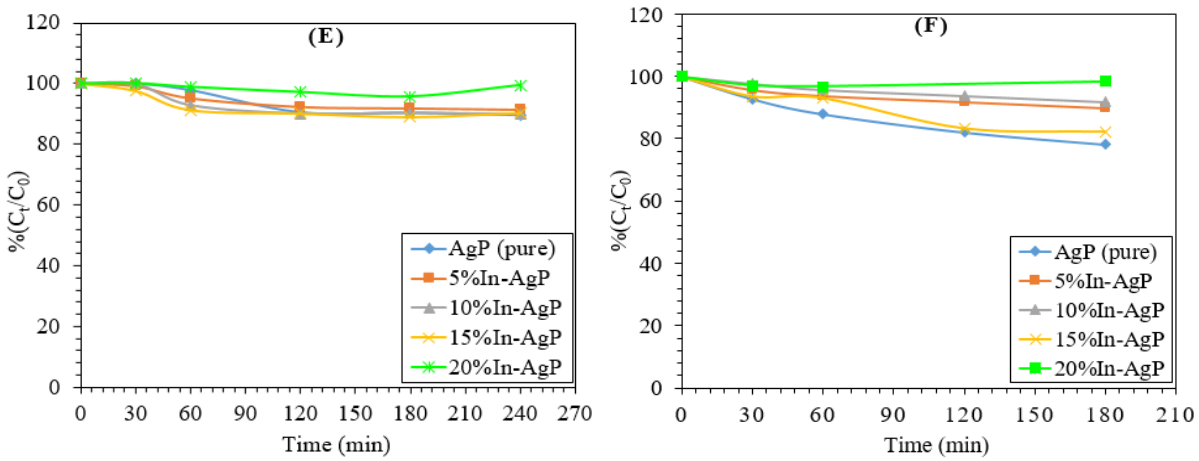


**Fig.5.** Adsorption kinetic of dyes on different catalysts; (A) MO + pH=7, (B) AO + pH=7, (C) MO + pH=4, (D) AO + pH=4, (E) MO + pH=10, (F) AO + pH=10

3.5.2. Photocatalytic degradation

Fig.6 ((A) and (B)) shows the results of photodegradation tests at pH=7. The variation in dyes concentration in term of % $C_t/C_0$ is presented as a function of the irradiation time. For MO, pure AgP is always better than the doped samples, more than 94% is degraded in 30 min with a rate constant of 0.092 $min^{-1}$. This rate is much faster than that observed for $TiO_2$ photocatalysts. However, the substituted samples reach the same amount of degradation in 3 h. On the other hand, 95% of AO is degraded in equal parts by pure and 20% In-AgP in 120 min, followed by 10% In-AgP and 15% In-AgP in 180 min.

At the initial pH solution equal to 4 (Fig.6 (C) and (D)), the adsorption is still negligible. The degradation efficiency of MO on In-doped semiconductors improved much more advantageously compared to virgin AgP, and 10% In-AgP showed the best activity with a yield of 99 % in 30 min, followed by complete degradation on 5% In-AgP and 20% In-AgP in 60 min. The same for AO photodegradation, but, this time the degradation efficiency of 15% In-AgP and 20% In-AgP was too close to that of 10% In-AgP and 91 %, 92 % and 93 % were respectively degraded in 120 min. The highest rate constant for MO degradation at pH = 4 corresponds to 10% In-AgP with a value of 0.0856 $min^{-1}$. However, for AO degradation, close rate constants of 0.0214 $min^{-1}$ and 0.0216 $min^{-1}$ were obtained for 10% In-AgP and 20% In-AgP, respectively.

At pH = 10 (Fig.6 (E) and (F)), 5% In-AgP was better for the degradation of the two dyes with 86 % in 30 min for MO and 83 % for AO at the same length of time with constant

rates of 0.0652 $min^{-1}$ and 0.0513 $min^{-1}$ respectively, followed by pure AgP, then the others come in last row.

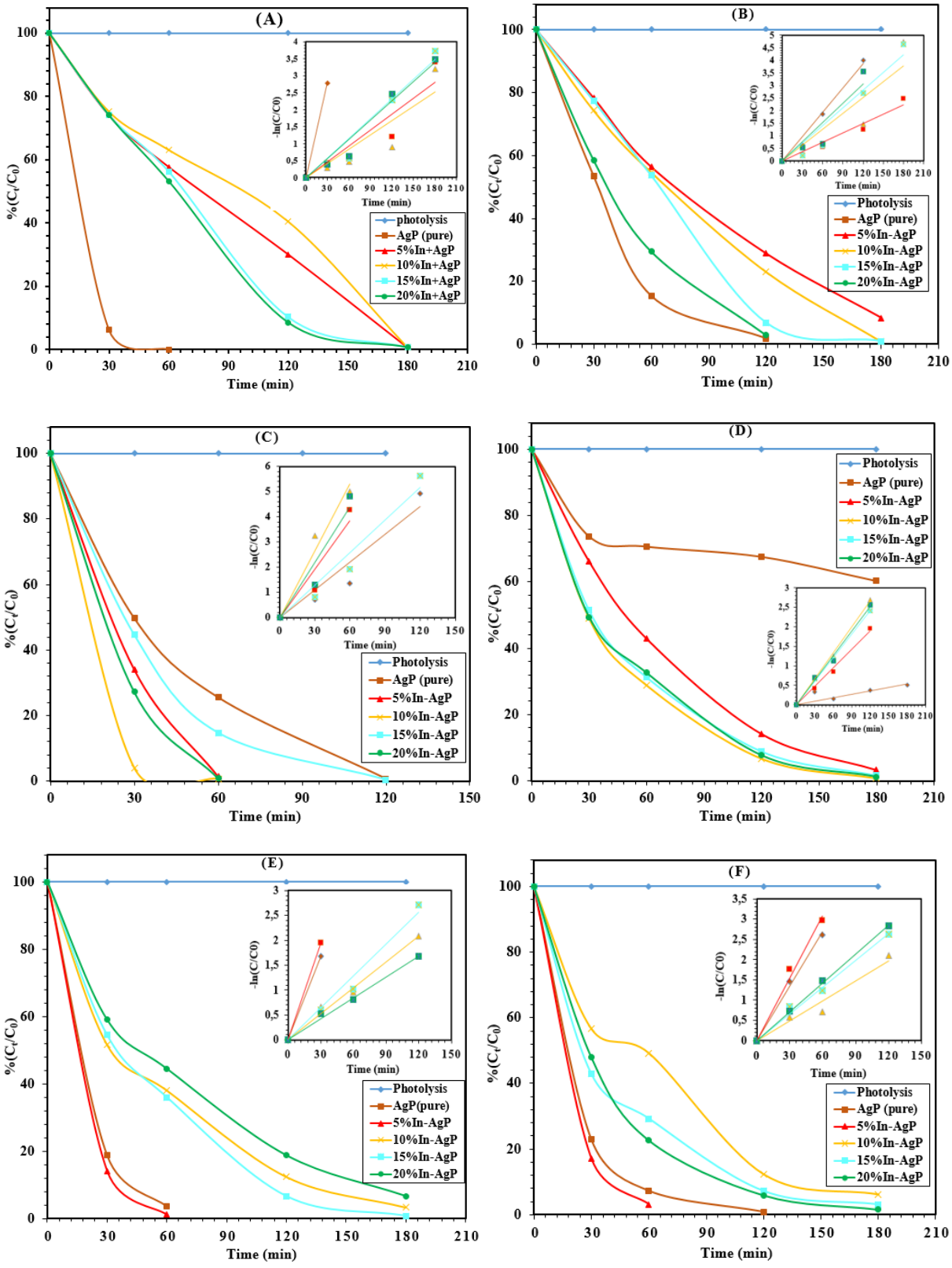

**Fig.6.** Photocatalytic degradation kinetic at pH=7((A) MO, (B) AO); pH=4 ((C) MO and (D) AO); pH=10 ((E) MO and (F) AO)

The conclusions that can be drawn from these results are, on the one hand, silver phosphate, whether doped or not, is more selective towards MO than to AO. This selectivity can be justified by the attractive forces between $Ag^+$ and the anionic charge of the MO dye which facilitates the contact between the dye and the catalyst thus leading to faster degradation. However, the same positive charge carried by the AO and the substrate causes repulsion between them, therefore, the contact is disadvantageous, thus the degradation takes longer time. But, if this is true, why did AO adsorb more than MO, taking in consideration that the adsorption of both dyes is so negligible? This could therefore lead us to conclude that adsorption is not a determining factor in the photodegradation procedure. The second conclusion that can be extracted is that all samples doped with $In^{3+}$ are more active than pure AgP in an acidic medium.

It is worthy to mention an important remark, all the previous reports agreed that silver phosphate is a highly active catalyst under visible light irradiation, but the barriers of its application are its instability and partial dissociation in solution. Though, through our works with this material we wound up to conclude that its photocatalytic activity could be considered as an indirect activity. By that we mean that its high activity, in fact is due to the free $Ag^+$ in the solution that released by the material when suspended in the solution. So, the challenge is to find ways that could stabilize $Ag^+$ cations in AgP structure. The reason for the observed reduction in the degradation kinetics after the incorporation of $In^{3+}$ in our current study could be the stabilization of the $Ag^+$ cations in the structure and therefore much less free $Ag^+$ cations in the solution. According to the previous DRX results, when $In^{3+}$ cations substituted $Ag^+$ cations in the silver phosphate lattice, the peaks were deflected to the left (lower 2θ). In addition, there is a decrease in the intensity of the peaks with the increasing dosage of indium cations. These results can be explained as follows, on the one hand the disorder of the crystal increases thus causing the decrease of the intensities, and on the other hand the structure underwent a slight contraction compared to the pure phase. All of these changes have taken place without transforming the centered cubic structure of the pure material. We assume that the disorder and shrinkage occurring in the network limits the mobility of $Ag^+$, due to the decrease in migration pathways, thus leading to moderate release into solution. As already mentioned, $In^{3+}$ represents a smaller radius compared to $Ag^+$, which implies smaller lattice parameters and subsequently minimalist structural changes and hence improved stability with the growth of cycling number.

In-doped AgP samples are more active than pure AgP in acidic medium. Indeed, the presence of $H^+$ in the solution contributes to the degradation. As well as, $In^{3+}$ cations play a key role of electron acceptor which prevents electron-hole recombination (Fig.7 (A)). These electrons can reduce the protons $H^+$ present in the solution to H· radicals. This active element contributes to the formation of hydroxyl (·OH) radicals and hydroperoxide ($HO_2$·) [42], which are powerful species in the photodegradation process. 10% In-AgP with the smallest particle diameter and minimal OH defects, is the most active among them. This could be justified by the fact that, the density of presence of OH groups on the other catalysts lead to their protonation by $H^+$ and therefore the efficiency is reduced because the related groups hamper the inductive effect of OH [39], on one hand. And on the other hand they obstruct the contact between the target polluting molecule and the catalyst (Fig.7 (B)), thus, the separation efficiency of the photogenerated electron-holes will be reduced, subsequently the photocatalytic activity will undergo a decrease. Moreover, we observed that the grains of these samples agglomerated during the photocatalytic test.

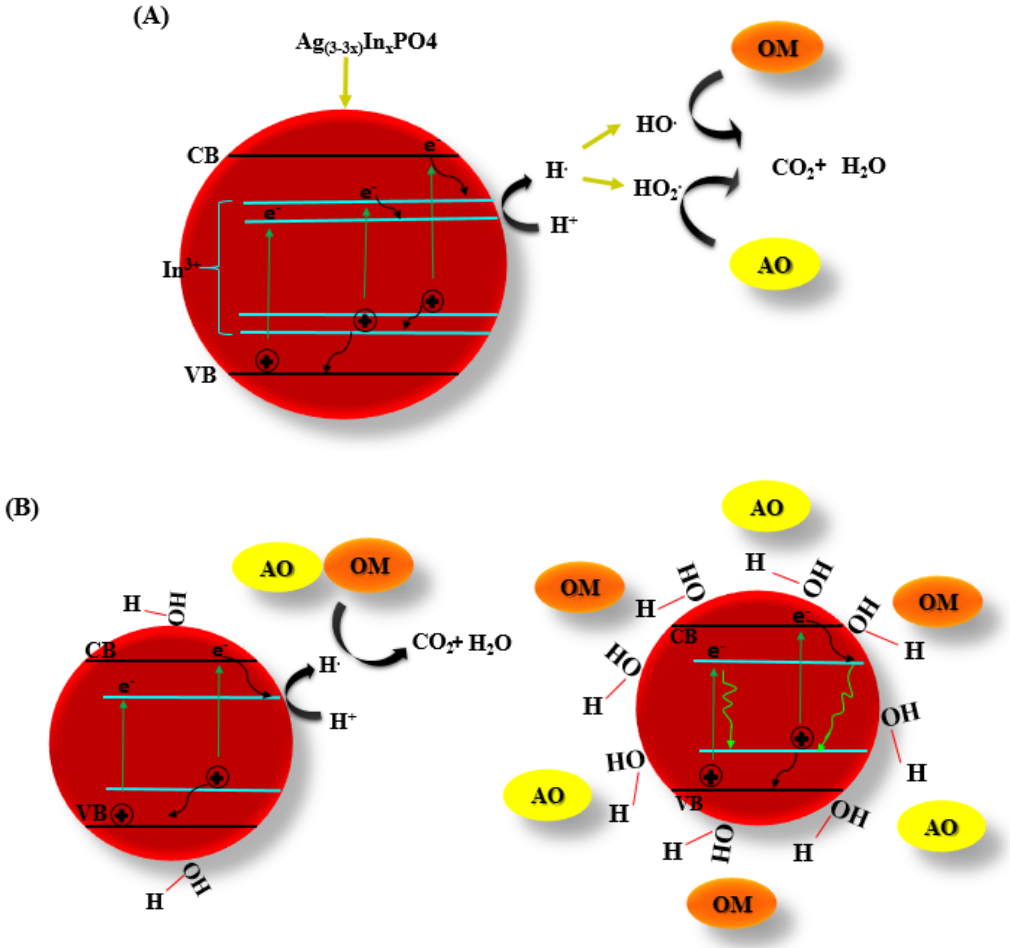

**Fig.7.** (A) Illustration of the electron-hole recombination prevention by indium cations; (B) Difference in photocatalytic performances explanation

### 3.5.3. Effect of scavengers

In order to propose a reactional mechanism and understand the role of different species in the degradation reaction, experiments with involved scavengers were carried out. As it is well-known the main active species in the degradation mechanism are the holes ($h^+$), hydroxyl radicals ($HO\cdot$) and superoxide anion radicals ($O_2^{-\cdot}$), yet, these latter are not used directly in the photocatalytic degradation, but, converted into $HO\cdot$ in aqueous medium [24]. To identify the strongest form in the degradation of both cationic and anionic dyes, $HO\cdot$ radical's scavenger isopropyl alcohol (IPA) and holes scavenger ethylenediaminetetraacetic acid (EDTA) were added to MO and AO degradation system with presence of both 10%In-AgP and AgP each one in the pH of activity in order to know if the pH has an effect on the active species. As presented in the Fig.8, for all samples and both dyes, the addition of EDTA inhibit severely the degradation of pollutants. In contrary, the addition of IPA displays a slight influence which is not even remarkable on the degradation. This result means that the holes are the major active species in the photocatalytic degradation of MO and AO by all catalysts.

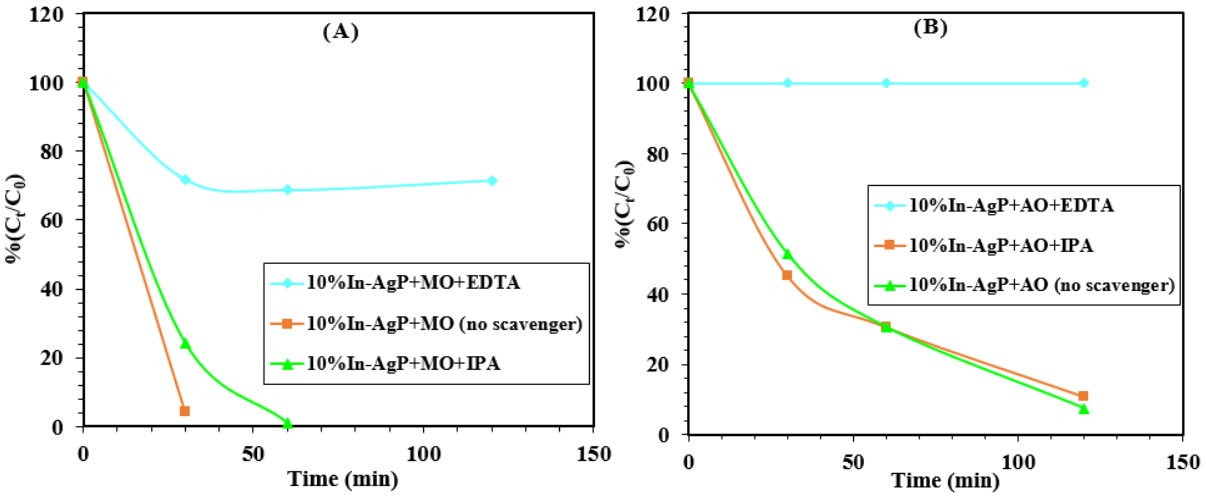

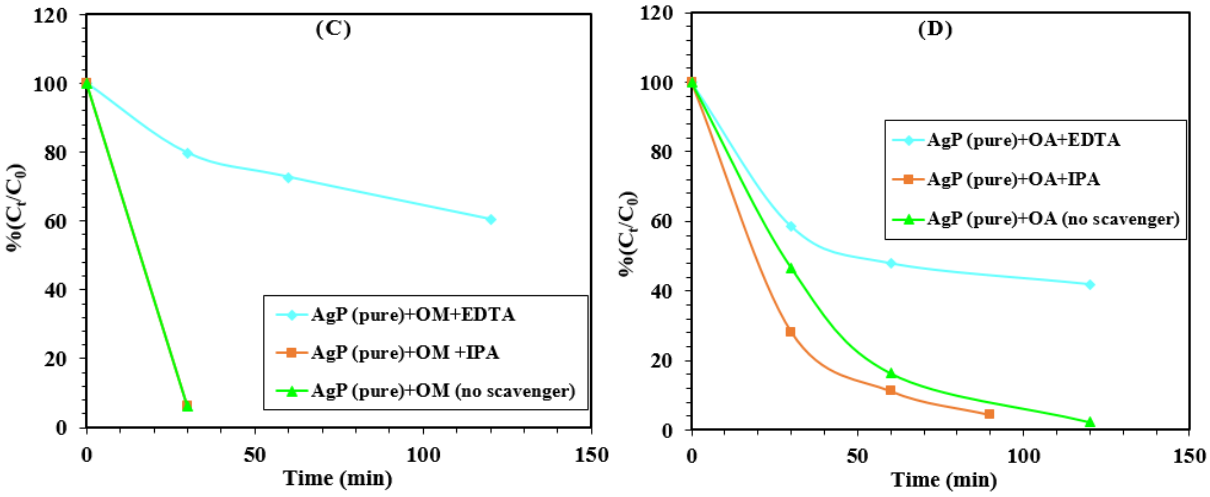


**Fig.8.** Effect of different scavengers on the kinetics of degradation of (A) MO and (B) AO by 10%In-AgP and by AgP (C) MO and (D) AO

3.5.4. Photocatalysts reusability

In order to fully assess photocatalytic activity, the reusability of a material is an important factor for having a place in the industrial application. In order to explore the stability of synthesized materials, recycling tests were performed on the best photocatalyst (10%In-AgP) and the pure AgP material for further comparison. As shown in Fig.9, after five cycles, the photocatalytic performances of AgP gradually decreased with the increasing number of cycles, from 93.91% in the first cycle to 63% in the last cycle. In contrast, 10% In-AgP not only maintain its high photocatalytic performance, but has also improved (over 99 %). This amelioration could be justified by the formation of metallic Ag and argentite ($Ag_2O$) particles on the surface of AgP. Since In-AgP is more stable than pure AgP, a very low quantity of $Ag^+$ transfers to the solution. During exposure to irradiation, $Ag^+$ is reduced by the excited electrons to metal Ag, a part of Ag could be oxidized, giving birth to $Ag_2O$ particles. The synergetic effect of these three materials enhances the use of visible light. But, with the growth of cycling numbers, the amount of Ag and $Ag_2O$ increases and covers the entire surface, a fact that negatively affects the light absorption capacity of AgP. As a result, the photocatalytic activity will be reduced.

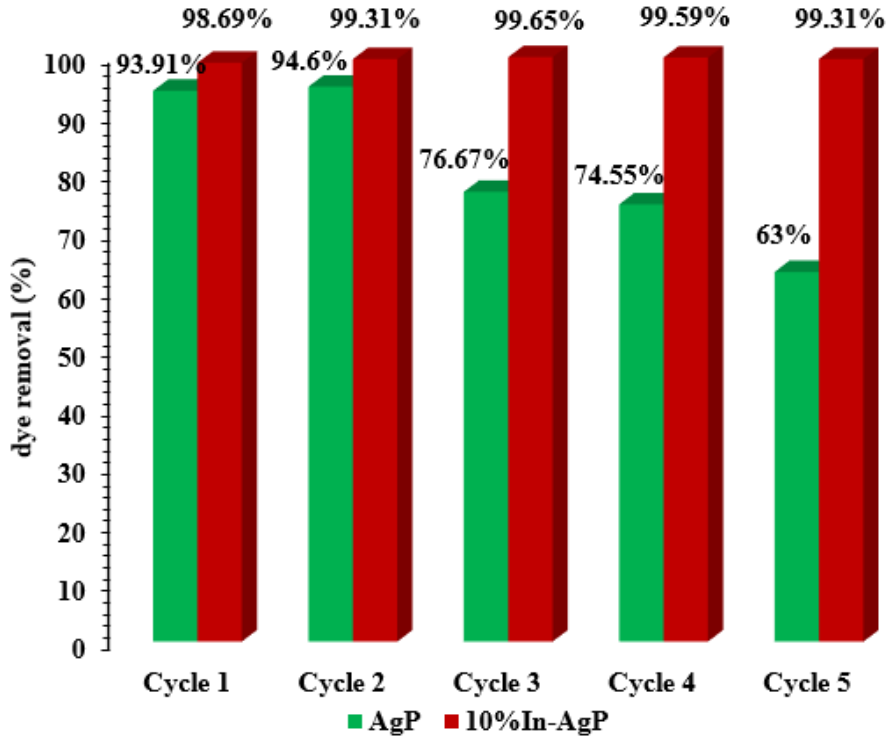


**Fig.9.** Cycling runs of MO photodegradation over **AgP and** 10%In-AgP

## Conclusion

A series of indium (5, 10, 15, and 20 w %) doped $Ag_3PO_4$ was synthesized by a co-precipitation. The presence of indium in the materials was confirmed by DRX, SEM/EDX, and FTIR. The spherical morphology of AgP was well preserved after doping, apart from the fact that the particle diameter decreased compared to pure material. As well as In cations peaks appear in EDX data and become more intense with increasing dosage. Substitution by indium does not affect the centered cubic phase of the starting materials, only the parameters of the unit cells undergo a slight reduction. The incorporation of indium into the structure advantageously improved the stability of AgP and prevented the severe release of $Ag^+$ cations in the solution, knowing that the free cations have an important role in the degradation, therefore, after the incorporation of indium the degradation kinetics were somewhat restricted compared to the pure phase. The degradation procedure was carried out in three media of different pH. The doped samples were very active at acidic pH, assuming that $H^+$ protons contribute to the degradation, and 10% In-AgP with the minimum OH defect and the smallest particle's diameter, showed elevated photodegradation activity against methyl orange and auramine O. Moreover, $In^{3+}$ did not alter the selectivity of AgP and it remains the same for all materials and it is favored towards MO than towards AO. In addition, we ended up finding that the holes are the powerful

active species in the degradation of the two dyes. Finally, the interesting result after the substitution with indium is the improvement in the stability of silver phosphate, after 5 cycles the degradability is still greater than 99%.

**References**


[1] R. Vinu and G. Madras, "Environmental remediation by photocatalysis," *J. Indian Inst. Sci.*, vol. 90, no. 2, pp. 189–230, 2010.

[2] A. Fujishima and K. Honda, "Electrochemical Evidence For Mechanism of the Primary Stage of Photosynthesis," *Bull. Chem. Soc. Jpn.*, vol. 44, no. 4. pp. 1148–1150, 1971.

[3] A. Di Paola, E. García-López, G. Marcì, and L. Palmisano, "A survey of photocatalytic materials for environmental remediation," *J. Hazard. Mater.*, vol. 211–212, pp. 3–29, 2012, doi: 10.1016/j.jhazmat.2011.11.050.

[4] M. Iwasaki, M. Hara, H. Kawada, H. Tada, and S. Ito, "Cobalt ion-doped TiO2 photocatalyst response to visible light," *J. Colloid Interface Sci.*, vol. 224, no. 1, pp. 202–204, 2000, doi: 10.1006/jcis.1999.6694.

[5] S. Kim, S. J. Hwang, and W. Choi, "Visible light active platinum-ion-doped TiO2 photocatalyst," *J. Phys. Chem. B*, vol. 109, no. 51, pp. 24260–24267, 2005, doi: 10.1021/jp055278y.

[6] S. Klosek and D. Raftery, "Visible Light Driven V-Doped TiO2 Photocatalyst and Its Photooxidation of Ethanol," *J. Phys. Chem. B*, vol. 105, no. 14, pp. 2815–2819, 2001.

[7] T. J. P. Kishore Sridharan, Eunyong Jang, "Novel visible light active graphitic C3N4-TiO2 composite photocatalyst : Synergistic synthesis , growth and ...," *Appl. Catal. B Environ.*, vol. 142– 143, pp. 718– 728, 2013.

[8] M. Machida, K. Norimoto, and T. Watanabe, "The effect of SiO2 addition in super-hydrophilic property of TiO2 photocatalyst," *J. Mater. Sci.*, vol. 34, pp. 2569–2574, 1999.

[9] H. Zhao, F. Su, X. Fan, H. Yu, D. Wu, and X. Quan, "Graphene-TiO 2 composite photocatalyst with enhanced photocatalytic performance," *Chinese J. Catal.*, vol. 33, no. 5, pp. 777–782, 2012, doi: 10.1016/S1872-2067(11)60374-4.

[10] and S.-F. Y. Lang Chen, Rui Huang, Miao Xiong, Qing Yuan, Jie He, Jing Jia, Meng-Yuan Yao, Sheng-Lian Luo, Chak-Tong Au, "Room-temperature synthesis of flower-

like BiOX (X=Cl, Br, I) hierarchical structures and their visible-light photocatalytic activity," *Inorg. Chem.*, vol. 52, no. 19, pp. 11118–11125, 2013, doi: 10.1021/ic401349j.

[11] L. Ge, C. Han, X. Xiao, and L. Guo, "Synthesis and characterization of composite visible light active photocatalysts MoS2-g-C3N4 with enhanced hydrogen evolution activity," *Int. J. Hydrogen Energy*, vol. 38, no. 17, pp. 6960–6969, 2013, doi: 10.1016/j.ijhydene.2013.04.006.

[12] J. Yu, J. Xiong, B. Cheng, Y. Yu, and J. Wang, "Hydrothermal preparation and visible-light photocatalytic activity of Bi2WO6 powders," *J. Solid State Chem.*, vol. 178, no. 6, pp. 1968–1972, 2005, doi: 10.1016/j.jssc.2005.04.003.

[13] X. Hu and C. Hu, "Preparation and visible-light photocatalytic activity of Ag3VO4 powders," *J. Solid State Chem.*, vol. 180, no. 2, pp. 725–732, 2007, doi: 10.1016/j.jssc.2006.11.032.

[14] Z. Yi *et al.*, "An orthophosphate semiconductor with photooxidation properties under visible-light irradiation," *Nat. Mater.*, vol. 9, no. 7, pp. 559–564, 2010, doi: 10.1038/nmat2780.

[15] W. Shi, F. Guo, and S. Yuan, "In situ synthesis of Z-scheme Ag3PO4/CuBi2O4 photocatalysts and enhanced photocatalytic performance for the degradation of tetracycline under visible light irradiation," *Appl. Catal. B Environ.*, vol. 209, pp. 720–728, 2017, doi: 10.1016/j.apcatb.2017.03.048.

[16] C. Tang, E. Liu, J. Wan, X. Hu, and J. Fan, "Co3O4 nanoparticles decorated Ag3PO4 tetrapods as an efficient visible-light-driven heterojunction photocatalyst," *Appl. Catal. B Environ.*, vol. 181, pp. 707–715, 2016, doi: 10.1016/j.apcatb.2015.08.045.

[17] W. Liu, M. Wang, C. Xu, S. Chen, and X. Fu, "Ag3PO4/ZnO: An efficient visible-light-sensitized composite with its application in photocatalytic degradation of Rhodamine B," *Mater. Res. Bull.*, vol. 48, no. 1, pp. 106–113, 2013, doi: 10.1016/j.materresbull.2012.10.015.

[18] H. Katsumata, T. Sakai, T. Suzuki, and S. Kaneco, "Highly efficient photocatalytic activity of g-C3N 4/Ag3PO4 hybrid photocatalysts through z-scheme photocatalytic mechanism under visible light," *Ind. Eng. Chem. Res.*, vol. 53, no. 19, pp. 8018–8025, 2014, doi: 10.1021/ie5012036.

[19] Q. Cao, L. Xiao, J. Li, C. Cao, S. Li, and J. Wang, “Morphology-controlled fabrication of Ag 3 PO 4 / chitosan nanocomposites with enhanced visible-light photocatalytic performance using different molecular weight chitosan,” *Powder Technol.*, vol. 292, pp. 186–194, 2016, doi: 10.1016/j.powtec.2016.02.003.

[20] N. Mohaghegh, E. Rahimi, and M. R. Gholami, “Ag3PO4/BiPO4 p-n heterojunction nanocomposite prepared in room-temperature ionic liquid medium with improved photocatalytic activity,” *Mater. Sci. Semicond. Process.*, vol. 39, pp. 506–514, 2015, doi: 10.1016/j.mssp.2015.05.066.

[21] Y. Bi, S. Ouyang, J. Cao, and J. Ye, “Facile synthesis of rhombic dodecahedral AgX/Ag3PO4 (X = Cl, Br, I) heterocrystals with enhanced photocatalytic properties and stabilities,” *Phys. Chem. Chem. Phys.*, vol. 13, no. 21, pp. 10071–10075, 2011, doi: 10.1039/c1cp20488b.

[22] L. Liu *et al.*, “A stable Ag3PO4@PANI core@shell hybrid: Enrichment photocatalytic degradation with π-π conjugation,” *Appl. Catal. B Environ.*, 2016, doi: 10.1016/j.apcatb.2016.08.005.

[23] L. Xu, W. Q. Huang, L. L. Wang, G. F. Huang, and P. Peng, “Mechanism of superior visible-light photocatalytic activity and stability of hybrid Ag3PO4/graphene nanocomposite,” *J. Phys. Chem. C*, vol. 118, no. 24, pp. 12972–12979, 2014, doi: 10.1021/jp5034273.

[24] S. Zhang, S. Zhang, and L. Song, “Super-high activity of Bi3+ doped Ag3PO4 and enhanced photocatalytic mechanism,” *Appl. Catal. B Environ.*, vol. 152–153, pp. 129–139, 2014, doi: 10.1016/j.apcatb.2014.01.020.

[25] M. S. A. Hussien and I. S. Yahia, “Fabrication progress of selective and durable Ni 2 + -doped Ag 3 PO 4 for visible-light degradation of various textile dyes,” *J. Photochem. Photobiol. A Chem.*, vol. 368, pp. 210–218, 2019, doi: 10.1016/j.jphotochem.2018.09.051.

[26] L. Song, Z. Chen, T. Li, and S. Zhang, “A novel Ni2+-doped Ag3PO4 photocatalyst with high photocatalytic activity and enhancement mechanism,” *Mater. Chem. Phys.*, vol. 186, pp. 271–279, 2017, doi: 10.1016/j.matchemphys.2016.10.053.

[27] M. S. A. Hussien and I. S. Yahia, “Visible photocatalytic performance of nanostructured molybdenum-doped Ag3PO4: Doping approach,” *J. Photochem.*

*Photobiol. A Chem.*, vol. 356, pp. 587–594, 2018, doi: 10.1016/j.jphotochem.2018.01.026.

[28] A. B. Trench *et al.*, "Rational Design of W - Doped Ag 3 PO 4 as an E ffi cient Antibacterial Agent and Photocatalyst for Organic Pollutant Degradation," *ACS Omega*, vol. 5, p. 23808−23821, 2020, doi: 10.1021/acsomega.0c03019.

[29] H. Yu, H. Kang, Z. Jiao, G. Lü, and Y. Bi, "Tunable photocatalytic selectivity and stability of Ba-doped Ag3PO4 hollow nanosheets," *Chinese J. Catal.*, vol. 36, no. 9, pp. 1587–1595, 2015, doi: 10.1016/S1872-2067(15)60938-X.

[30] Y. P. Xie and G. S. Wang, "Visible light responsive porous Lanthanum-doped Ag3PO4 photocatalyst with high photocatalytic water oxidation activity," *J. Colloid Interface Sci.*, vol. 430, pp. 1–5, 2014, doi: 10.1016/j.jcis.2014.05.020.

[31] M. Afif, U. Sulaeman, A. Riapanitra, R. Andreas, and S. Yin, "Use of Mn doping to suppress defect sites in Ag 3 PO 4 : Applications in photocatalysis," *Appl. Surf. Sci.*, vol. 466, pp. 352–357, 2019, doi: 10.1016/j.apsusc.2018.10.049.

[32] E. Ghazalian, N. Ghasemi, and A. R. Amani-Ghadim, "Enhanced visible light photocatalytic performance of Ag3PO4 through doping by different trivalent Lanthanide cations," *Mater. Res. Bull.*, vol. 88, pp. 23–32, 2016, doi: 10.1016/j.materresbull.2016.11.036.

[33] E. Ghazalian, N. Ghasemi, and A. R. Amani-Ghadim, "Effect of gadollunium doping on visible light photocatalytic performance of Ag3PO4: Evaluation of activity in degradation of an anthraquinone dye and mechanism study," *J. Mol. Catal. A Chem.*, vol. 426, pp. 257–270, 2016, doi: 10.1016/j.molcata.2016.11.026.

[34] P. Dong, H. Li, and L. Han, "Shape-controllable synthesis and morphology-dependent photocatalytic properties of Ag3PO4 crystals," *J. Mater. Chem. A*, vol. 1, pp. 4651–4656, 2013, doi: 10.1039/C3TA00130J.

[35] T. Yan *et al.*, "Improving the photocatalytic performance of silver phosphate by thermal annealing : In fl uence of acetate species," *J. Alloys Compd.*, vol. 680, pp. 436–445, 2016, doi: 10.1016/j.jallcom.2016.04.142.

[36] J. F. Cruz-Filho *et al.*, "Effect of different synthesis methods on the morphology, optical behavior, and superior photocatalytic performances of Ag 3 PO 4 sub-microcrystals using white-light-emitting diodes," *J. Photochem. Photobiol. A Chem.*,

vol. 377, pp. 14–25, 2019, doi: 10.1016/j.jphotochem.2019.03.031.

[37] H. Agbe, N. Raza, D. Dodoo-Arhin, A. Chauhan, and R. V. Kumar, “H2O2 rejuvenation-mediated synthesis of stable mixed-morphology Ag3PO4 photocatalysts,” *Heliyon*, vol. 4, no. 4, p. e00599, 2018, doi: 10.1016/j.heliyon.2018.e00599.

[38] X. Guan, J. Shi, and L. Guo, “Ag3PO4 photocatalyst: Hydrothermal preparation and enhanced O2 evolution under visible-light irradiation,” *Int. J. Hydrogen Energy*, vol. 38, pp. 11870–11877, 2013, doi: 10.1016/j.ijhydene.2013.07.017.

[39] R. Li, X. Song, Y. Huang, Y. Fang, M. Jia, and W. Ma, “Visible-light photocatalytic degradation of azo dyes in water by Ag 3 PO 4 : An unusual dependency between adsorption and the degradation rate on pH value 1,” *"Journal Mol. Catal. A Chem.*, vol. 421, pp. 57–65, 2016, doi: 10.1016/j.molcata.2016.05.009.

[40] J. Zhao, Z. Ji, C. Xu, X. Shen, L. Ma, and X. Liu, “Hydrothermal syntheses of silver phosphate nanostructures and their photocatalytic performance for organic pollutant degradation,” *Cryst. Res. Technol.*, vol. 49, no. 12, pp. 975–981, 2014, doi: 10.1002/crat.201400298.

[41] C. Wang *et al.*, “A facile one-step solvothermal synthesis of bismuth phosphate-graphene nanocomposites with enhanced photocatalytic activity,” *J. Colloid Interface Sci.*, vol. 435, pp. 156–163, 2014, doi: 10.1016/j.jcis.2014.06.031.

[42] S. Abbasi and M. Hasanpour, “Variation of the photocatalytic performance of decorated MWCNTs (MWCNTs-ZnO) with pH for photo degradation of methyl orange,” *J. Mater. Sci. Mater. Electron.*, vol. 28, no. 16, pp. 11846–11855, 2017, doi: 10.1007/s10854-017-6992-5.